Supplementary information and figures

High-throughput tracking of single yeast cells in a microfluidic imaging matrix

Didier Falconnet, Antti Niemistö, Robert James Taylor, Marketa Ricicova, Tim Galitski, Ilya Shmulevich, Carl Hansen.

Supplementary Video 1:
Live-cell imaging (DIC mode) of wild-type yeast exposed to 100nM alpha-factor.

Supplementary Video 2:
Live-cell imaging (Fluorescence mode) of wild-type yeast exposed to 100nM alpha-factor.

Supplementary Video 3:
Live-cell imaging (frames alternating between DIC and Fluorescence mode) of wild-type yeast exposed to 100nM alpha-factor.

Supplementary Video 4:
Live-cell imaging (DIC mode) of wild-type yeast exposed to 5nM alpha-factor.

Supplementary Video 5:
Live-cell imaging (frames alternating between DIC and Fluorescence mode) of wild-type yeast exposed to 5nM alpha-factor.
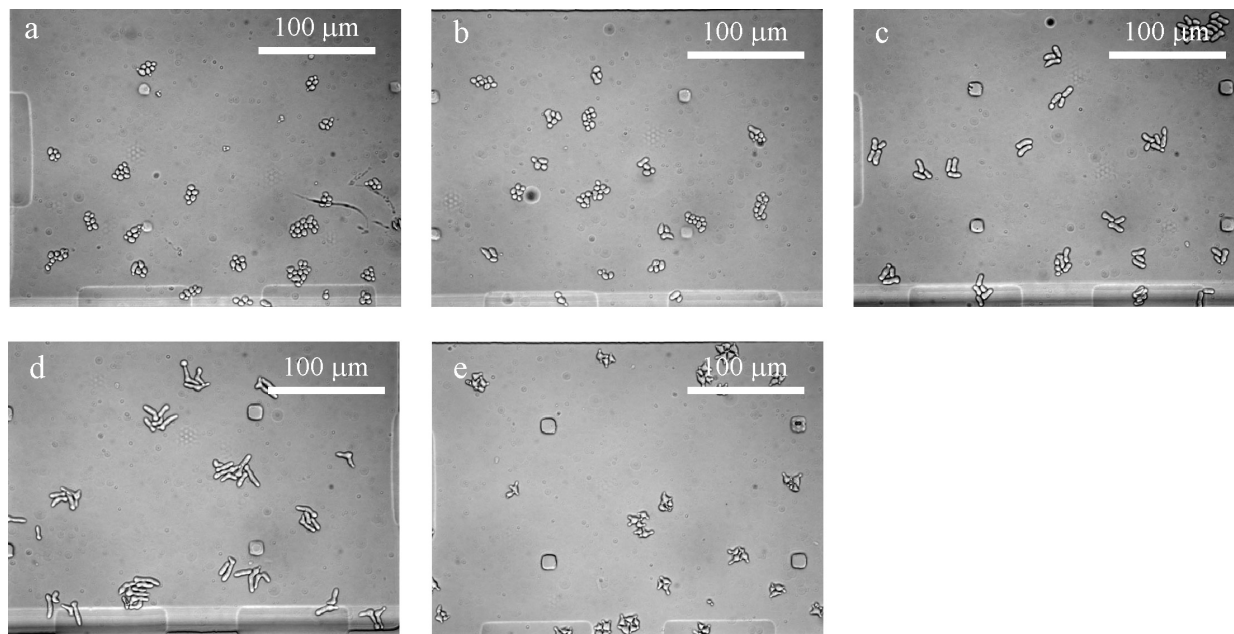
Supplementary Figure 1: Yeast morphologies observed under various pheromone concentrations.

Supplementary Figure 1: Morphologies observed for cells exposed to a range of pheromone concentrations. (a) 3 nM: cells have budding yeast morphologies and divide normally. (b) 5 nM: a fraction of cells elongate and growth arrest. (c) 8 nM: all the cells growth arrest and form elongations. (d) 14 nM: cells become highly elongated with length 4 times longer than their width. (e) 100 nM: at saturating concentrations cells display shmooing morphologies with one or multiple shmoos.

Supplementary Figure 2: The image acquisition and analysis pipeline

**Image acquisition
and data storage**

**Cell segmentation
Generation of movies (MPEG)**

Figure calculation
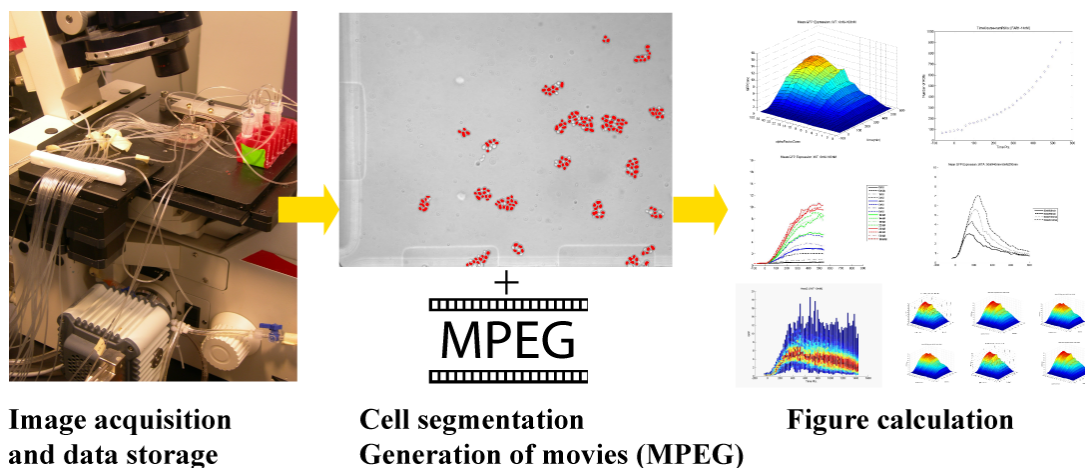
Supplementary Figure 2: The 128 chambers of the chip are imaged periodically in brightfield and fluorescence generating 512 images per run (2 fields of view per chamber with a brightfield and fluorescent pair of images per field of view). In a typical experiment the whole chip is imaged every 20 min during 24 hours, generating 36,864 images representing about 100 Gb that are saved in an external hard drive. Image acquisition is automated in Labview (National Instruments).

We developed the analysis pipeline in Matlab (Mathworks) to perform cell segmentation, cell labeling and data presentation. Furthermore, movies are generated for each chamber from the raw tiff images as brightfield and fluorescent sequences or combination of both.

Supplementary Figure 3: Cell segmentation algorithm
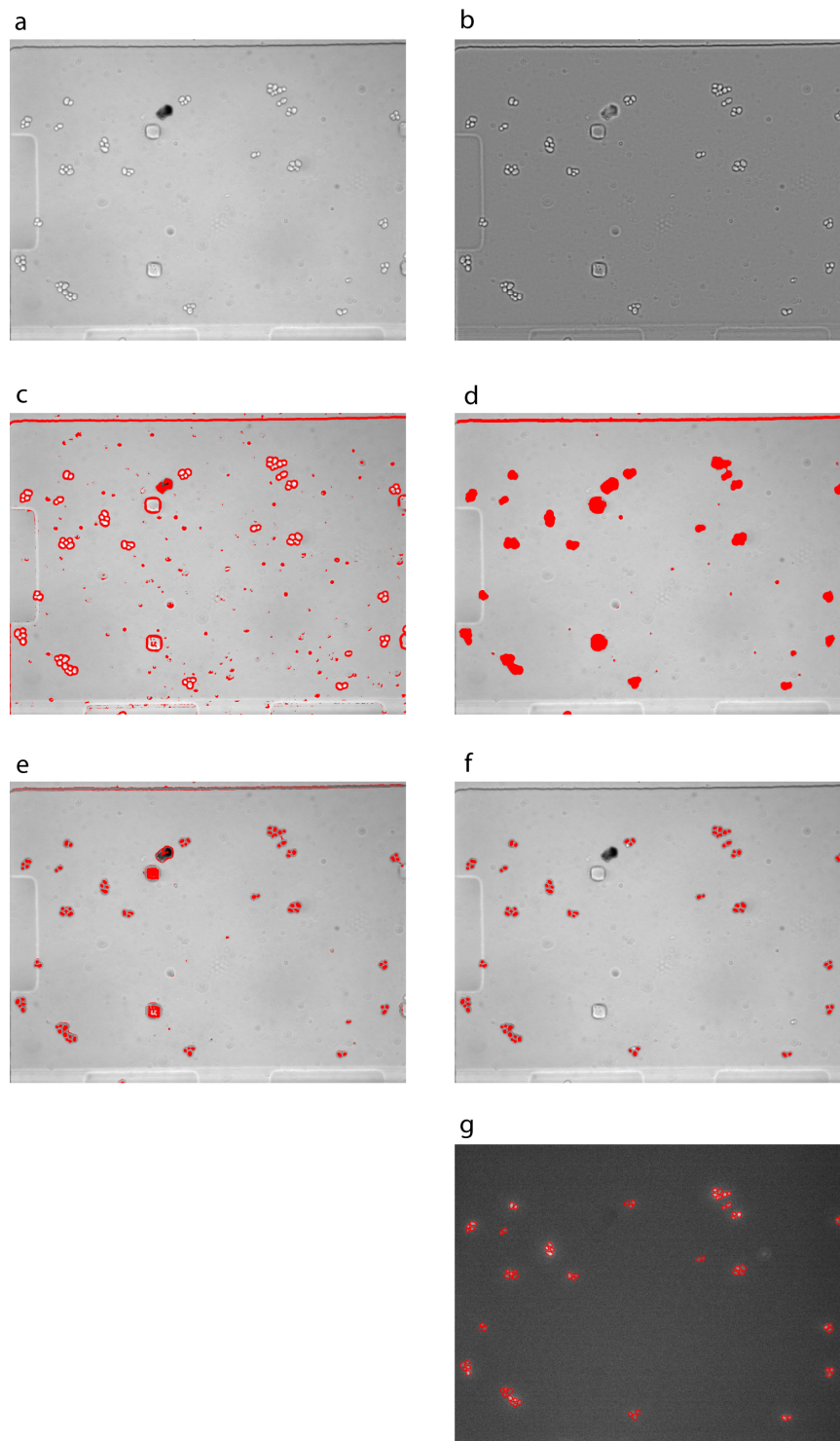
Supplementary figure 3: The sequence performed by the algorithm to segment the cells.

Supplementary Figure 4: Microscope setup
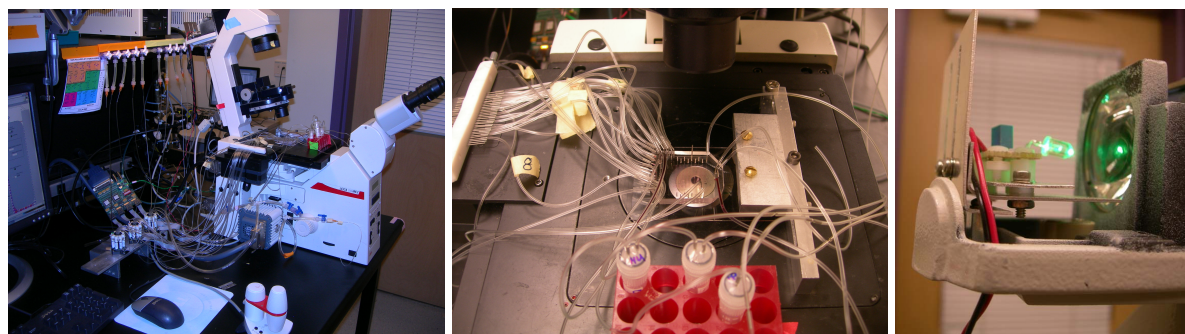
Supplementary figure 4: (Left) a view of the complete setup. (Centre) Image of chip clamped on the stage with a custom aluminum holder, media bottles for perfusion, tubing connections necessary for pneumatic actuation of control valves. (Right) A picture of our adapted microscope; the original halogen brightfield light source was replaced with an LED emitting in the pass-band of the fluorescence emission filter, thus allowing for ms switching between brightfield and fluorescence image acquisition without a shutter.

Supplementary Figure 5: Closing a channel with a push-down valve
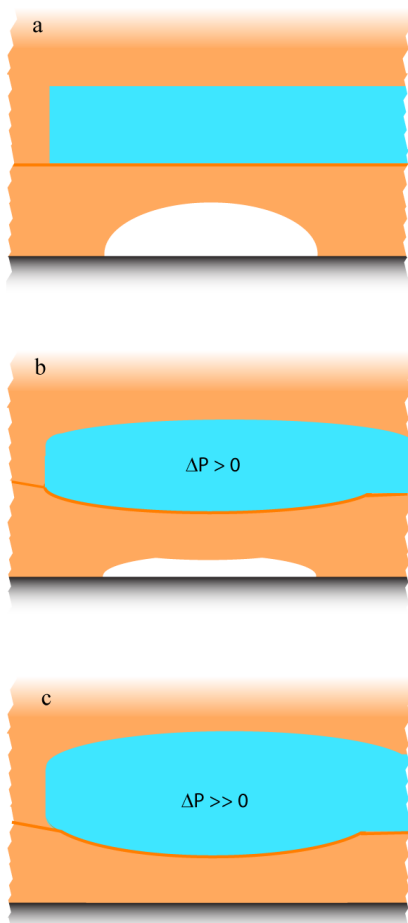
Supplementary figure 5: The flow layer containing the flow channels for cells and media (white) is bonded to the glass slide. The control layer is above the flow layer and results in a push-down valving geometry. The control channel (the valve in blue) is filled with water and when pressurized (typically 30 psi) deflects the thin PDMS membrane to fully close the flow channel.

Supplementary Figure 6: Perfusion protocol for 16 independent rows and diffusion kinetics.
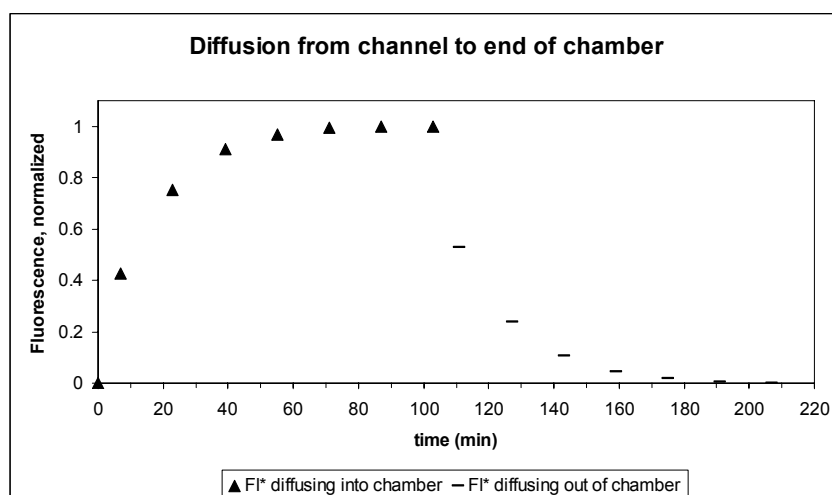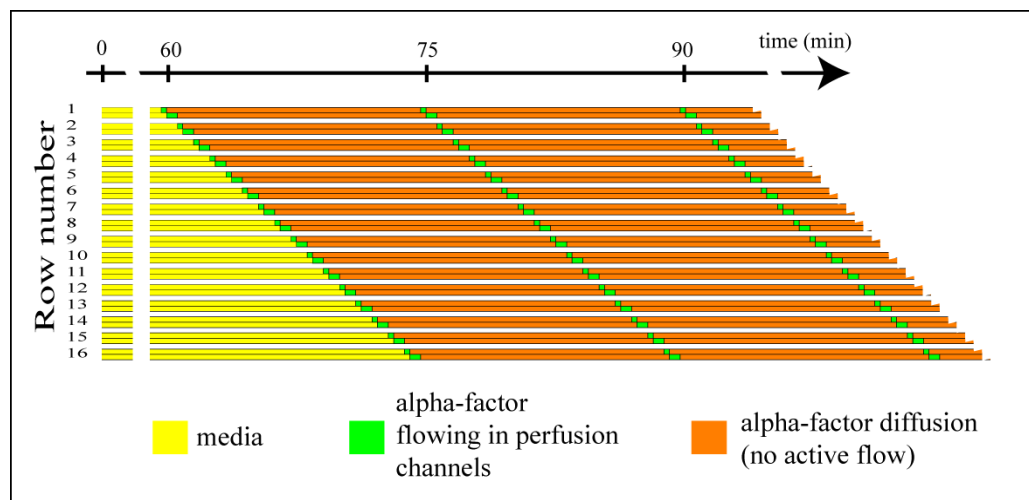
Supplementary figure 6: (a) Each row is perfused for 35 s with a pre-programmed alpha-factor concentration (table 2) every 16 min. 35 s allows for complete volume exchange of the perfusion channel. Prior to perfusion across row the binary tree is primed through a dedicated waste channel (one for each row) to avoid cross-contamination between adjacent rows of the array. The perfusion channel remains closed while its corresponding waste channel is open for a 15 s priming step. 15 s is enough to replace the volume of the binary tree between the chemical inlets and the beginning of the row of interest. (b) Fluorescence signal at the back of a chamber when the 16 row perfusion protocol (a) was applied. The exponential fluorescent signal decrease could be observed upon switching from the fluorescein solution to media.

Supplementary Methods

Image analysis pipeline

To analyze the large number of images per experiment, we built a customized image analysis pipeline using MATLAB software (The Mathworks, Inc, Natick, MA). The core of the pipeline consisted of cell segmentation, cell tracking, and enhanced green fluorescence protein (EGFP) concentration calculation. These three major steps are described below and graphically summarized in **Supplementary figure 1**.

Cell segmentation

The DIC image shown in Supplementary figure 3a is used to illustrate the cell segmentation steps. The image was first enhanced using background subtraction. The background was estimated by spatially averaging the image using a 21×21 mean filter. The resulting image is shown in Supplementary figure 3b. The first step in cell segmentation identified the cell walls. Yeast cell walls were clearly visible as continuous borders that were darker than the background, giving two useful properties: the local mean was low and the local variance was high. Cell wall pixels were marked as those pixels whose local mean was below a threshold T_m and whose variance was above a threshold T_v [1]. A 5×5 neighborhood was used to calculate the local mean and variance. The threshold T_m was set to $\mu_m - 1/2 \, \sigma_m$, where μ_m and σ_m were the global mean and standard deviation of the local mean image respectively. Similarly, the threshold T_v was set to $\mu_v + 1/3 \, \sigma_v$, where μ_v and σ_v were the global mean and standard deviation of the local variance image respectively. Cell wall segmentation was finalized by filling some of the small holes inside the detected cell walls with a morphological closing by a 5×5 structuring element. The result is shown in Supplementary figure 3c. The next step of the segmentation method is to find a mask of cell areas. This was done by applying the following sequence of operations to the local variance image: threshold with the threshold obtained by Otsu's method [2] multiplied by 0.5, dilate by a circular structuring element inside a 11×11 square, fill holes inside the objects, and erode with the same circular structuring element. The result is shown in Supplementary figure 3d. The detected cell walls were then removed from the mask (Supplementary figure 3e). Following that, the objects in the resultant image were filled. Due to false negatives in cell wall detection, some cells were incorrectly grouped together and recognized as a single cell. These were separated from each other with the watershed of the Euclidean distance function of the complement image [3]. The h-maxima transformation with h set to 0.75 was used in order to prevent over-segmentation. Finally, objects that were smaller than 30 pixels or larger than 800 pixels in size were excluded. The final cell segmentation result is shown in Supplementary figures 3f and 2g.

Cell tracking

The cell tracking problem was posed in terms of combinatorial optimization as the classic assignment problem. Cells from the image frame at time point t acted as the agents, cells from the image frame at time point t-1 acted as tasks, and the cost of assigning a task to an agent was equal to the Euclidean distance between the respective cells from time points t and t-1. The centroid locations of each cell were found for each time point (image frame). A cost matrix, C, can then be calculated for each pair of consecutive frames, such that C_{ij} is the distance between the cell with

the label i in the frame at t-1 and the cell with the label j in the frame at t. Assuming N cells at both time points, we have an N×N cost matrix, and the one-to-one mapping between cells at the two time points with the lowest sum of costs can be found using the Hungarian algorithm [4]. In that case, cell tracking can be performed for a sequence of images by simply iterating the Hungarian algorithm until all time points have been processed. However, since we are dealing with live cells undergoing cell division, the number of cells increases between time points. Moreover, the segmentation step produces some false negatives, which means that the tracking algorithm needs to be able to cope with cells not being present at some time points, but reappearing later on. False positives, on the other hand, should not be assigned to correctly segmented cells from the previous time point. To help cope with the changing number of cells, we tracked the cells in the reverse order, that is, starting from the last time point. That way, we give a label to each cell that is present in the time series at the initialization of the tracking algorithm. Because the Hungarian algorithm requires a square weight matrix, but the changing number of cells results in non-square weight matrices, we add infinity-valued columns to the weight matrix to make it square, when necessary, and use an implementation of the Hungarian algorithm that does not use these infinity valued columns in the solution of the assignment problem. In addition, we added the following mechanisms to cope with the challenges listed above:

Outlier removal: Due to the microfluidic chip design, segmented objects that are far away from any cell location in the previous frame are likely to be false positives. Therefore, objects whose Euclidean distance to the nearest cell from the previous frame is greater than 50 pixels are removed before applying the Hungarian algorithm.

Retiring labels: If a label was not seen in two consecutive frames, it was put on a list of retired labels so that it would not be used again. At each iteration, the elements of the cost matrix corresponding to retired labels were set to infinity before applying the Hungarian algorithm.

Zeroing unlikely assignments: After applying the Hungarian algorithm, the cost vector corresponding to the solution of the assignment problem was analyzed using robust statistics. Outlying assignments were removed. In other words, assignments that were associated with a much larger cost than others were considered as false assignments.

Keeping current position if cell is missing: If a cell from the previous frame was not assigned to a cell in the current frame, the locations of the cells from the previous frame were used as the cell locations of the previous frame for the next iteration as well. This enabled the tracking algorithm to assign cells from frame t-2 to cells from frame t even if the cell was missing in the intermediate frame t-1, due to a false negative in the segmentation of that frame.

New label issuing: A new label was issued for each cell for which no cell from the previous frame was assigned.

Occasionally false positive and false positive segmentation occurred and they were manually corrected for using a custom-built MATLAB editing tool.

Measurement of EGFP concentration

Because of the unevenness of the fluorescent excitation field the images were corrected for shading (flat field correction) using the method of M. A. Model and J. K. Burkhardt [5].

$$x_{corrected} = 1000 \times \frac{x_{raw} - \langle x'_{raw} \rangle}{x_{standard} - x_{blank}} \qquad \text{Eq S1}$$

Where x_{raw} is the fluorescent image containing the cells (raw image), $x_{standard}$ corresponds to a standard fluorescent image acquired before each experiment. The standard slide was made by putting a 5 µl drop of a fluorescein solution onto a slide (identical to the slides supporting the microfluidic chips) and covered with a microscope cover-slip. This image shows how even the field of excitation is. The image was spatially averaged using a 15×15 mean filter. x_{blank} is an image of the slide without anything on it. This image is used to correct for the slide autofluorescence and the camera noise. $<x'_{raw}>$ is the mean value of pixels in x_{raw} that are not bounded to any regions identified from the segmentation algorithms. All the three images were obtained under the same conditions. The factor 1000 merely scales the corrected image so that the values are in a convenient range.

The total fluorescence of each cell was summed from the corrected image pixel values bounded by the segmented regions identified from the segmentation algorithms. For each cell, the EGFP concentration was obtained by dividing the total cellular fluorescence intensity by a volume estimate for the cell. The volume estimate was based on the cross-sectional cell area that was obtained from the cell segmentation result, and calculated using the "conical" method as described previously [6].

Generating movies from each chamber

MATLAB scripts were built to construct time-lapse imaging movies for each chamber in brightfield, fluorescent, or combined imaging formats.

Biological constructs

The full list of strains is given in Supplementary Table 1. Deletion mutants were obtained from the Open Biosystems Yeast Knockout (YKO) collection, as was the wild type (WT) BY4714 strain. All strains are derived from the parental S288C strain and have the following base genotype: MATa *his3Δ1 leu2Δ0 met15Δ0 ura3Δ0*. Deletion mutants in the YKO collection were derived using a polymerase chain reaction (PCR) based strategy to replace the open reading frame with a KanMX deletion cassette. We confirmed each deletion using PCR methods. To report on mating-pathway-dependent gene expression we transformed the strains with the gene coding for enhanced green fluorescent protein (GFP) under control of a mating-specific promoter. The promoter consisted of 3 consecutive pheromone response elements (PREs) from the PRM1 promoter, plus 3 flanking PRM1 promoter bases on each side, plus a CYC1 core promoter placed just prior to the ATG start site. The PRE-promoter-GFP construct (PRE-GFP) was placed adjacent to the *HIS3* selection element using the Longtine *et al.* cassettes [7] and integrated at the *his3Δ1* locus using flanking sequences introduced by long-oligo PCR. The integration was verified by PCR. In each strain the pheromone protease gene, *BAR1*, was deleted to preclude complications resulting from genotype-dependent Bar1 activity. The *BAR1* coding sequence was deleted using PCR methods with the pFA6a-hphNTI hygromycin cassette as described in Janke *et al* [8].

WT	*MATa leu2Δ 0 met15Δ 0 ura3Δ 0 bar1Δ*::HphNT2 *his3*::PRE-GFP-*HIS3*
far1Δ	*MATa leu2Δ 0 met15Δ 0 ura3Δ 0 bar1Δ*::HphNT2 *his3*::PRE-GFP-*HIS3 far1Δ*::KanMX4
fus3Δ	*MATa leu2Δ 0 met15Δ 0 ura3Δ 0 bar1Δ*::HphNT2 *his3*::PRE-GFP-*HIS3 fus3Δ*::KanMX4
kss1Δ	*MATa leu2Δ 0 met15Δ 0 ura3Δ 0 bar1Δ*::HphNT2 *his3*::PRE-GFP-*HIS3 kss1Δ*::KanMX4
msg5Δ	*MATa leu2Δ 0 met15Δ 0 ura3Δ 0 bar1Δ*::HphNT2 *his3*::PRE-GFP-*HIS3 msg5Δ*::KanMX4

ptp2Δ   MATa leu2Δ 0 met15Δ 0 ura3Δ 0 bar1Δ::HphNT2 his3::PRE-GFP-HIS3 ptp2Δ::KanMX4
slt2Δ   MATa leu2Δ 0 met15Δ 0 ura3Δ 0 bar1Δ::HphNT2 his3::PRE-GFP-HIS3 slt2Δ::KanMX4
ste50Δ   MATa leu2Δ 0 met15Δ 0 ura3Δ 0 bar1Δ::HphNT2 his3::PRE-GFP-HIS3 ste50Δ::KanMX4

Table 1. Details of the strains used in this study.

Materials and media

The inlet ports of the chip were punched with a manual punching press (Schmidt Technology press, Germany converted for punching holes by Technical Innovations Inc., USA) with cylindrical punch bits (Technical Innovations Inc., USA .035 x .025 x 1.5 304 SS TiN Coated).
The chip was interfaced with the world via stainless steel pins of 0.025 OD x 0.017 ID, 0.500" length (New England small tubes Corp, USA, PN 1310-02). Tygon tubes were supplied by Cole-Parmer, USA. The stock solutions feeding the chip were stored in custom adapted pressurized 2 ml microtube bottles (Sarstedt, Germany). Stainless steels pins were pushed through the cap and sealed with epoxy glue on the outside of the bottle. Each bottle was pressurized with 8-10 psi air.

The glass slides were cleaned in an ultrasound bath (Branson 5510, 40 kHz) for 3h in ultra-pure water (18 MΩ *cm).

To covalently bond the chip to the glass slides we performed an oxygen plasma surface treatment (Harrick plasma-cleaner PDC 32G). The PDMS chip and the glass slide were placed in the center of the chamber with both surfaces to be bonded facing up. The chamber was flushed with pure oxygen and pumped down twice before inducing the plasma for 10 s at a power of 18 W. Upon venting both surfaces were brought into contact immediately and a gentle pressure on the chip to initiate bonding.

Cell culture and agarose gel preparation

Cells were grown overnight in 5 ml YPD in a spinner at 30°C. The next morning 50 ul of stationary phase cell suspension was diluted into 5 ml of synthetic complete media with 2% dextrose (SCD) supplemented with 20 mg/ml of BSA (Sigma Aldrich) and grown to exponential phase at 30°C until OD_{600} of 0.8-1. Cells were spun down (5000 rpm, 2 min in a Microfuge 18 centrifuge with a radius of approx. 6 cm) and concentrated to an OD_{600} between 2 and 4 depending on the desired seeding density. The 1.5 ml vials containing the cells were placed on a heating block at 30°C.
The agarose powder (Sigma A2576, Type IX-A) was dissolved in SCD at 2.8% w/v. Vigorous magnetic stirring and boiling in a *bain-marie* completely dissolved the agarose within 5 min. The vial was allowed to cool to 30°C.
To each cell suspension vial we added the equivalent amount of gel in a 1:1 ratio leading to an OD of 1 or 2 depending on the initial density and a final gel of 1.4%. We found that it was more accurate to add the appropriate mass of agarose rather than volume due to the difficulty to accurately pipette slightly viscous solutions. Each vial was vortexed for 20 s and placed back into the heating block. The agarose gel used has an ultra-low gelling temperature (<17°C) and keeping it at 30°C helped keep its viscosity low. Prior to loading the cells the vials were extensively vortexed and guaranteed homogeneous suspensions.

About 3 ul of cell suspension were sucked into a tygon tube equipped with a stainless steel pin with the help of a 1 ml syringe and plugged into the cell inlet port of the chip. The line was pressurized with 8-10 psi in order to push the cell suspension through the column of the chip. Each strain was sequentially loaded in the chip with this process. Upon completion the pressure was released and the valves portioning the chambers were actuated.

Live-cell imaging

Each of the 128 chambers is imaged by two fields of view in bright-field and in fluorescence.

To decrease the acquisition time for imaging a complete chip we replaced the halogen bulb (for bright-field) with an ultra-bright green light emitting diode (LED 5000ucd, 3.5 V with a bulb size 1.3/4, PN95B1796, Newark, USA). The diode allowed for rapid ON and OFF switching (automatically controlled by our Labview image acquisition software). The fluorescent excitation was kept ON while acquiring the bright-field image.

Time to image the 128 chambers was essentially limited by the speed of the motorized stage. We believe that improved hardware could reduce the time to approximately 5 min if higher temporal resolution would be desired. Alternatively, subsets of the matrix may be imaged at higher temporal resolution if required.

Microfluidic devices were mounted onto a Leica DMIRE2 fluorescent microscope and cells were imaged with a 40x air objective (Leica HCX, long working distance, FLUOTAR PL with correction collar, NA=0.6) (**Supplementary figure 4**). High-throughput image acquisition was accomplished using simultaneous custom control of a motorized XYZ stage and an ORCA-ER digital camera (Hamamatsu Photonics, Hamamatsu Japan). All fluidic control software was developed using LabVIEW (National Instruments) software. The x-y-z position of each chamber was recorded in a semi-automated manner prior to launch the automated image acquisition and was completed in about 15 min. In order to prevent any chip movement during the experiment we drilled and threaded holes in the automated microscope stage to accommodate a custom made chip-clamping device (Supplementary figure 4, centre).

Cellular fluorescence was excited using an external light source connected to the microscope with liquid light guide (Leica EL6000). A Leica filter cube L5 (BP 480/40, BP 527/30 nm) was used to excite and visualize the GFP molecules. Differential interference contrast (DIC) and fluorescent images were captured with a 100 ms and 700 ms exposure respectively, and binning of 1 was used. Two light polarizing filters were in the light paths, one behind the LED and one before the CCD camera. Each of the 128 chambers was acquired in two fields of view, giving a total of 256 DIC / fluorescent image pairs (total 512 images) acquired per time point. Images had a resolution of 1344×1024 pixels. This setup allowed imaging the whole chip in 9 min. For most experiments a 20 min sampling period was sufficient.

During the entire course of the experiment the device was isolated from light and kept at a temperature of 25°C ± 1°C.

PDMS Chip fabrication details

The microfluidic chip consists of 3 layers: control layer with pneumatic valves, flow layer with chambers and flow channels, and a glass slide. Control layer and flow layer were fabricated from two components of PDMS, RTV A and RTV B, in different ratios. The control layer was mixed at a 5A:1B ratio, poured on the control mold wafer, degassed in vacuum for approximately 45 min

and baked at 80ºC for 60min. The flow layer was prepared at a 20A:1B ratio, poured on the flow mold wafer, spun at 2300rpm for 60s and baked at 80ºC for 45min. The control layer was then peeled off the silicon wafer and aligned with the flow layer. Both layers were baked together again for 1 hour to promote bonding and then the combined device was peeled off the flow wafer. After punching holes for all flow and control layer connections the chip was baked overnight and plasma bonded to a glass slide.

Chip architecture and operations

The chip layer containing the valves is placed above the flow layer used to perfuse and load the cells. This results in a push-down [9] valving geometry, described in **Supplementary figure 5**. The valve lines are dead-end filled with di-H_2O and actuated at 30 psi. Dead-end filling is performed in a few seconds owing to the high gas permeability of PDMS [10].

Channels directly connected to a row of 8 chambers are referred to as perfusion channels. Each of the 16 perfusion channels has a complementary waste channel located above the chamber (Figure 1a and 1b). The chip has a 16 pairs of perfusion and waste channels totaling 32 rows. A multiplexing valve architecture is used to control each row independently or in combinations. Each row is connected to the chemical inlets (Figure 1a, region 3) with equal length fluidic path via a binary tree to ensure identical flow conditions for each row. This binary tree structure has the advantage of having no "dead-volume" which usually leads to fluid cross-contamination.[9] The number of valve lines (V_N) required for N flow channel scales with $V_N = 2Log_2(N)$. In our case only 10 valve lines are required to control 32 flow channels. A de-multiplexer is used at the end of the channels to guide the flow to a waste. The valves are computer controlled (Labview custom interface) by miniature pneumatic solenoid valves (Lee Valve Co, Charlotte, NC) assembled on an eight-valve manifold (Fluidigm Corp., San Francisco, CA) which are connected to the NI card via a break-out board (Fluidigm, Inc, CA). Instructions, electronics designs, and drive software for making solenoid actuators are available at http://thebigone.stanford.edu/foundry/.

Any desired solution can simply be pushed with pressurized chemical lines into the desired rows by opening the proper chemical line control valves. However, arbitrary chemical formulations requires the on-chip mixing of stock solutions using an integrated peristaltic pump. An on-chip peristaltic pump is composed of 3 valves placed in series that can displace minute volumes if actuated in the proper sequence [9] (Figure 1a, region 6). The flow velocity depends on the volume beneath on valve and the pumping frequency. Velocities in the order of several mm/s can easily be achieved. By opening sequentially different chemical lines for defined numbers of pump cycles one can mix solutions very accurately as shown in Figure 1e of the paper. The rows were perfused with different concentrations of alpha-factor as listed in table 2.

Row	Pheromone concentrations	# pump cycle for ea. stock solution *based on 10 pump cycles*		
	[nM]	0nM	10 nM	100 nM
1	*0*	*10*		
2	*0*	*10*		
3	*1*	*9*	*1*	
4	*3*	*7*	*3*	
5	*4*	*6*	*4*	
6	*5*	*5*	*5*	
7	*6*	*4*	*6*	

8	8	2	8	
9	10		10	
10	14	5	4	1
11	18	1	8	1
12	22	6	2	2
13	30	7		3
14	40	6		4
15	50	5		5
16	100			10

Table 2. Chemical formulation for each row. Each train of 10 pump cycles was repeated for 35 s in each perfusion row before switching to the consecutive row and formulating its appropriate mixture.

Fig 2c in the paper demonstrates the mixing accuracy. We ran a similar protocol to the one shown in Table 2 but replaced pheromones with fluorescein in order to visualize the mixing accuracy. The plotted fluorescent signal was measured in the back of each chamber (greatest diffusion path) and the error bars indicate the standard deviation across the 8 chambers of each row (for identical regions of interests in each chamber). We attributed the subtle variations to differences in chamber heights resulting in variations in the thickness of fluorescein solution light path.

We measured the diffusion kinetics of fluorescein from the perfusion channels to the back of the chambers to estimate the time required to reach saturation equilibrium in the chambers. While under continuous perfusion of a fluorescein solution images were periodically acquired. Figure 1f shows that equilibrium was reached within 9 min. However, fluorescein is smaller (376 Da) than alpha-factor (1860 Da) and thus should diffuse faster. Diffusion time is inversely proportional to the Stokes radius of the diffusing molecule which itself scales with the cubic root of the molecular weight. Consequently the diffusion time (t) is proportional to the cubic root of the molecular weight (M_w):

$$t \propto (M_w)^{1/3}$$

Alpha-factor is 4.9 fold heavier than fluorescein resulting in an estimate of 1.7 fold increase in diffusion time. Hence, under continuous flow each chamber is saturated with alpha-factor in about 15 min. In experiments where each row was perfused with a different concentration of alpha-factor (Figure 3) the perfusion was periodic rather than continuous as represented in supplementary figure 6b. These show that chambers achieve 95% of the input concentration within approximately 60 min. In the current study we monitored the cells response over a much longer time scale (24 h) so this relatively slow stimulation was not a limiting factor. The longer equilibration time under periodic perfusion is due to depletion of the concentration of the perfusion channels during the 15 minute equilibration between perfusion cycles. In cases where faster modulation of the environment is required this delay can be removed by ensuring that the sections of diffusion channels in contact with the chambers have much larger volume than the chambers, resulting in the same behaviour as observed under continuous perfusion. Furthermore, faster molecule delivery to the cells under continuous flow can be achieved by shortening and widening the diffusion path. All proposed modifications can be implemented in a straight forward manner by adapting the CAD design and creating new molds for chip fabrication. We are currently revising the device geometries for this purpose.

Supplementary References

1   A. Niemisto, M. Nykter, T. Aho, H. Jalovaara, K. Marjanen, M. Ahdesmaki, P. Ruusuvuori, M. Tiainen, M. L. Linne, and O. Yli-Harja, *EURASIP J Bioinform Syst Biol*, 2007, 46150.

2   N. Otsu, *Ieee Transactions on Systems Man and Cybernetics*, 1979, **9**, 62-66.

3   P. Soille, *Morphological Image Analysis: Principles and Applications.* 2nd ed, Springer-Verlag. 2003.

4   H. W. Kuhn, *Naval Research Logistics*, 2005, **52**, 7-21.

5   M. A. Model and J. K. Burkhardt, *Cytometry*, 2001, **44**, 309-316.

6   A. Gordon, A. Colman-Lerner, T. E. Chin, K. R. Benjamin, R. C. Yu, and R. Brent, *Nat. Methods*, 2007, **4**, 175-181.

7   M. S. Longtine, A. McKenzie, D. J. Demarini, N. G. Shah, A. Wach, A. Brachat, P. Philippsen, and J. R. Pringle, *Yeast*, 1998, **14**, 953-961.

8   C. Janke, M. M. Magiera, N. Rathfelder, C. Taxis, S. Reber, H. Maekawa, A. Moreno-Borchart, G. Doenges, E. Schwob, E. Schiebel, and M. Knop, *Yeast*, 2004, **21**, 947-962.

9   J. Melin and S. R. Quake, *Annu. Rev. Biophys. Biomol. Struct.*, 2007, **36**, 213-231.

10   T. C. Merkel, V. I. Bondar, K. Nagai, B. D. Freeman, and I. Pinnau, *Journal of Polymer Science Part B-Polymer Physics*, 2000, **38**, 415-434.